World Academy of Science, Engineering and Technology
International Journal of Bioengineering and Life Sciences
Vol:8, No:2, 2014

A Nanosensor System Based On Disuccinimydyl–CYP2E1 for Amperometric Detection of the Anti-Tuberculosis Drug, Pyrazinamide

R. F. Ajayi, U. Sidwaba, U. Feleni, S. F. Douman, E. Nxusani, L. Wilson, C. Rassie, O. Tovide, P. G. L. Baker, S. L. Vilakazi, R. Tshikhudo, E. I. Iwuoha

Abstract**—**Pyrazinamide (PZA) is among the first-line pro-drugs in the tuberculosis (TB) combination chemotherapy used to treat *Mycobacterium tuberculosis*. Numerous reports have suggested that hepatotoxicity due to pyrazinamide in patients is due to inappropriate dosing. It is, therefore necessary to develop sensitive and reliable techniques for determining the PZA metabolic profile of diagnosed patients promptly and at point-of-care. This study reports the determination of PZA based on nanobiosensor systems developed from disuccinimidyl octanedioate modified Cytochrome P450-2E1 (CYP2E1) electrodeposited on gold substrates derivatised with (poly(8-anilino-1-napthalene sulphonic acid) PANSA/PVP-AgNPs nanocomposites. The rapid and sensitive amperometric PZA detection gave a dynamic linear range of 2μM to 16μM revealing a limit of detection of 0.044μM and a sensitivity of 1.38μA/μM. The Michaelis-Menten parameters; K_M, K_M^{app} and I_{MAX} were calculated to be 6.0μM, 1.41μM and $1.51x10^{-6}$ A, respectively, indicating a nanobiosensor suitable for use in serum.

Keywords**—**Cytochrome P450-2E1, Disuccinimidyl octanedioate, Pyrazinamide, Tuberculosis.

I. Introduction

TUBERCULOSIS (TB) is ranked second to HIV/AIDS among the burden of diseases faced by South Africa and remains a highly infectious disease worldwide [1]. The disease is caused by development of mycobacterium tuberculosis (MTB), a bacterium which affects the lungs, meninges, brain and spinal cord with the fully-developed diseases known as pulmonary-TB, TB meningitis, TB cerebritis, and TB myelitis, respectively. The bacterium has a dormant behavior which makes it very difficult to be detected at early stages and therefore has an impact on the incidences of multi-drug resistant TB (MDR-TB) and extensively drug-resistant TB (XDR-TB). Due to such effects, tuberculosis treatment is a multi-drug regimen consisting of first-line and second-line TB drugs, categorized according to their effectiveness against the bacteria [2].

The Sensor Lab of the University of the Western Cape, Mintek and the National Research Foundation of South Africa are greatly acknowledged for financial assistance to complete this study.

Rachel F. Ajayi, U. Sidwaba, U. Feleni, S. F. Douman, E. Nxusani, L. Wilson, C. Rassie, O. Tovide, P. G. L. Baker, and E. I. Iwuoha are with SensorLab at the Chemistry Department of the University of the Western Cape, Bellville, South Africa (phone: +2721-959-3049; fax: +2721-959-3055; e-mail: fngece@uwc.ac.za, eiwuoha@uwc.ac.za).

S. Vilakazi and R. Tshikhudo are with the Nanotechnology Innovation Centre, Advanced Materials Division, Mintek, Randburg, Johannesburg, South Africa.

Pyrazinamide (PZA) is among the first-line pro-drugs in the TB combination chemotherapy used in conjunction with rifampicin, ethambutol, and isoniazid [3]. For effective bacterium destruction, PZA (A in Fig. 1) has to be activated by enzymatic hydrolysis into pyrazinoic acid (POA) (B in Fig. 1) which possesses antibacterial activity against the old, slowly-replicating bacilli of mycobacterium tuberculosis that cannot be attacked by the other drugs [3], [4]. PZA is considered the most fundamental element in the TB therapy due to its sterilizing activity, and hence is responsible for shortening the therapy from the former nine months to the current six months duration [5]-[8]. Despite the remarkable advantages of PZA introduction in the therapy, such as its activity against replicating bacilli and sterilizing activity, there is little understanding on the mode of action of pyrazinamide which thrives in acidic environment which, in turn, leads to loss of pyrazinamiase activity. This behaviour is associated with the diverse mutations in the pncA encoding of pyrazinamidase, and is the main cause of MTB resistance to PZA [9], [10]. Also, this gene variation is the main source for the different metabolic categories where there are slow and fast metabolizers. The latter refers to patients whose metabolic rates are fast while the former refers to those whose rates are slow. These differences, together with the fixed dose inferred irrespective of metabolic profile, lead to greater chances of liver damage and hepatotoxicity induced by the accumulation of the drug and/or its metabolite. To reduce toxic levels of therapeutic drugs, regulatory bodies have set minimal inhibitory concentrations (MICs) with a MIC of 50–100 mg/L for PZA [11].

Although reports from bodies implemented to monitor TB (e.g. the DOTS, STOP-TB and TAC), have shown success in combating TB spread and recurrence, Tuberculosis remains a major health problem in South Africa. This is enhanced by factors such as over-crowding (since TB is a respiratory disease spread easily through coughing and breathing), and poor health seeking behavior (mainly in rural areas which constitute a larger population percentage), leading to delayed detection of diseases. Above all, the TB-HIV correlation plays a vital part with 73% of TB patients being HIV positive. Also, numerous reports have confirmed that PZA is responsible for hepatotoxicity amongst diagnosed patients [12]. Hence, there is increased demand for onsite analytical devices that can quantitatively and qualitatively allow monitoring of PZA (and other therapeutic drugs) with high sensitivity, selectivity and

faster response time and lower detection limits. Therefore, presented herein is rapid nanobiosensor system for the determination of PZA which is sensitive, has a reduced response time and the ability to allow for point-of-care analysis by studying the biotransformation of PZA in serum.

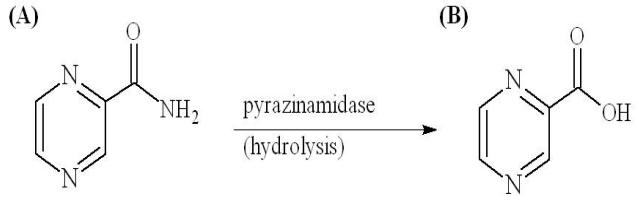

Fig. 1 Schematic presentation for the hydrolysis of (A) PZA into (B) PAO

II. Experimental Procedure

A. Synthesis of Nanocomposites

Enzyme modification was achieved as follows; 7.5mg of disuccinimidyl octanedioate (SA) was dissolved in a 125µL solution of 2.5% Dimethyl sulphoxide (DMSO) from which 5µL was reacted with 2µL of Cytochrome P450-2E1 (CYP2E1) dissolved in 50µL pH 7.4, 0.1M phosphate buffer solution. For 30min this reaction was allowed to take place at room temperature and was later terminated by adding 50µL of 0.1M cold Tris–HCl buffer pH 7.0. The resultant SA/CYP2E1 solution was stored refrigerated at -4ºC and was used within 3 days of preparation. For the purpose of this study, SA was used as a cross-linking agent between CYP2E1 and the nanocomposite silver nanoparticles/poly(8-anilino-1-napthalene sulphonic acid) (PANSA/PVP-AgNPs/) on Au electrodes. PANSA and PANSA/PVP-AgNPs were electrosynthesized and characterized using a previously reported procedure [13] but with minor adjustments. The development of the PZA nanobiosensor was achieved by immersing overnight the modified Au electrodes in a 10 mL buffer solution containing 30 µL of the SA/CYP2E1 mixture. The resultant Au/PVP-AgNPs/PANSA/SA-CYP2E1 nanobiosensor was rinsed thoroughly in buffer and stored refrigerated at -4 ºC when not in use. Electrochemical Impedance Spectroscopy (EIS), Transmission Electron Microscopy (TEM) and Atomic Force Microscopy (AFM) where used to interrogate the functionality of Au/PANSA/PVP-AgNPs/SA-CYP2E1.

B. Amperometric Detection of PYR using Au/PANSA/PVP-AgNPs/SA-CYP2E1

PZA standard solutions were prepared daily by dissolving finely ground PZA capsules in 50 mL pH 7.4, 0.1 M phosphate buffer solutions. The Au/PANSA/PVP-AgNPs/SA-CYP2E1 nanobiosensor was immersed in a 20 mL reaction cell containing the buffer solution where the concentration of PZA was varied. The determination of PZA was achieved under the following condition; CV and DPV experiments were carried out at a potential window of +300 mV to -800 mV, a sensitivity of 10 µA/V and scan rate of 20 mV/s. For the steady state amperometric determination the applied potential of -300 mV was chosen with stirring was maintained at 650 rpm using pH 7.4, 0.1 M phosphate buffer solution as the supporting electrolyte.

III. Results and Discussion

A. TEM Analysis

Fig. 2 indicates TEM images of PANSA/PVP-AgNPs/SA-CYP2E1 dispersed in methanol. Spherical and polydispersed silver nanoparticles with average diameter of 20 – 50 nm are seen attached onto the polymeric film seen as colourless while SA-CYP2E1, the white crystalline layers are seen attached onto both the polymeric film and silver nanoparticles. EDX analyses (not included) revealed the components of PANSA/PVP-AgNPs/CYP2E1 which are C-O-Fe-S-Ag from low to high energy respectively with energy scale of maximum approximately 7.5 keV. Observed therein was the presence of oxygen due to the ITO glass substrate components as well as sulphur contributed by the sulphonic substituent of PANSA. The presence of PVP-AgNPs was indicated by an optical absorption peak near 3 keV while the active site of CYP2E1 was indicated by the presence of Fe as optical peaks near 7.5 keV.

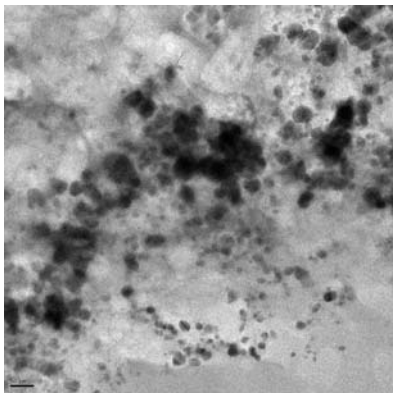

Fig. 2 TEM image of PANSA/PVP-AgNPs/SA-CYP2E1 nanocomposite

B. AFM Analyses

AFM analyses were carried out to investigate the differences in the surface morphologies of PANSA/PVP-AgNPs (Fig. 3 (a)) and PANSA/PVP-AgNPs/SA-CYP2E1 (Fig. 3 (b)). We observed that for the PANSA/PVP-AgNPs nanocomposite, the produced silver nanoparticles are almost homogenously distributed within the electrodeposited PANSA film whereas a rough and globular morphology was observed for PANSA/PVP-AgNP/SA-CYP2E1. The reason for the difference can be attributed to the highly hydrophilic nature of the polymer which is able to adsorb metal particles and forms rigid nanocomposites. In the presence of PANSA, the assembled silver nanoparticles are covered by PANSA evenly and thus prevent it from growing bigger. Moreover, PANSA adsorbed onto silver nanoparticles can also stabilize the formed silver nanoparticles, and with the electrodeposition of PANSA, silver nanoparticles can be entrapped into the PANSA film. The globular morphology observed for the

PANSA/PVP-AgNPs/CYP2E1 (Fig. 3 (b)) is consistent with the close packing of enzymes onto solid surfaces as reported by [14], [15]. This is indicative of the fact that the chemical modification of CYP2E1 did not drastically alter the morphology of PANSA/PVP-AgNPs.

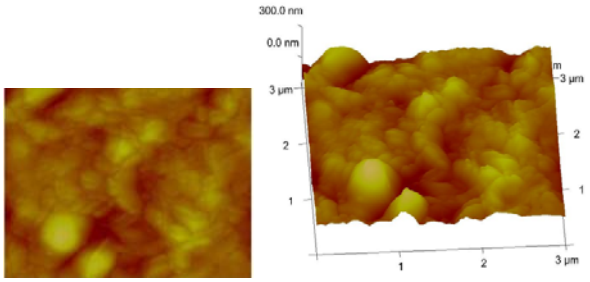

(a)

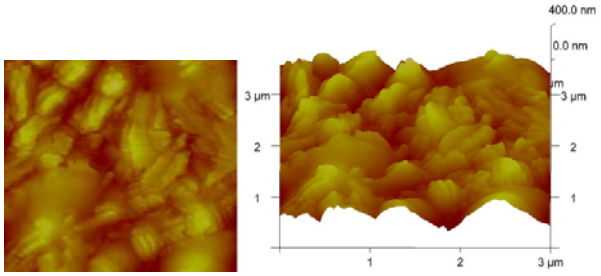

(b)

Fig. 3 1D and 3D AFM images of (a) PANSA/PVP-AgNPs (b) PANSA/PVP-AgNPs/SA-CYP2E1

C.EIS Analyses

EIS was chosen to monitor the assembly process achieved for the PZA nanobiosensor so as to obtain information between each step during the sensor development (Fig. 4). Fig. 5 is the Nyquist plot resultant during the development of the nanobiosensor. After assembling PVP-AgNPs onto PANSA films on Au surfaces (curve C), an increases semi-circle was observed (curve B). This is indicative of the partial semi-conductive nature of PVP-AgNPs whose conductivity is superior to that of PANSA. The successful adsorption of SA-CYP2E1 (curve A) onto the PANSA/PVP-AgNPs nanocomposites was denoted by an increased semicircle illustrating a slight restriction in the electron flow transfer between the Au electrode and the PANSA/PVP-AgNPs/SA-CYP2E1 nanobioelectrode [16], [17] indicating a slight reduction in conductivity. Therefore the direct interaction of the electrons with the bare Au electrode resulted in a (charge transfer resistance) R_{ct} value of 89.27 kohm whereas values for Au/PANSA/AgNPs (118 kohm), and Au/PANSA/PVP-AgNPs/SA-CYP2E1 (217.6 kohm) were also calculated.

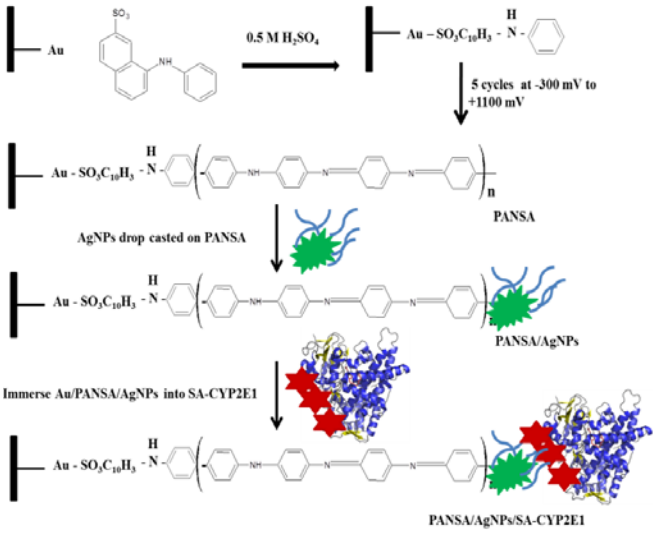

Fig. 4 Schematic representation of the steps involved in the development of the nanobiosensor system

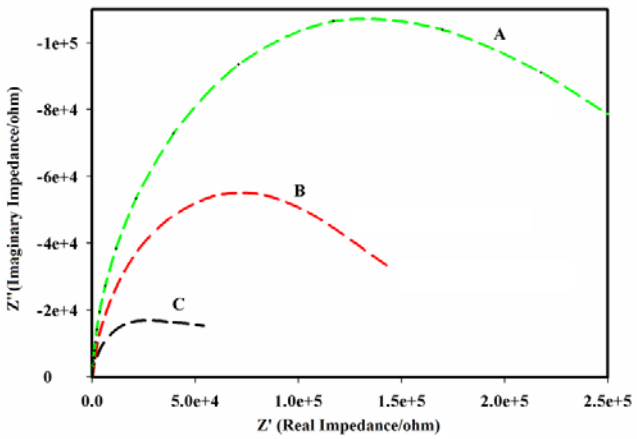

Fig. 5 EIS Nyquist plot of (A) Au/PANSA/PVP-AgNPs/SA-CYP2E1 nanobioelectrode, (B) Au/PANSA/PVP-AgNPs and (C) Au electrode

E. Electrocatalytic Reduction of PZA

Fig. 6 illustrates the CV responses of the Au/PANSA/PVP-AgNPs/SA-CYP2E1 nanobiosensor in the absence and presence of PZA at the low potential scan rate of 20 mV/s. Voltammograms obtained in the absence of PZA were performed in anaerobic solutions where only the electrochemistry of Au/PANSA/PVP-AgNPs essential for the oxidation and reduction of PVP-AgNPs and PANSA was observed. Illustrated in the diagram is a redox peak towards the more positive potentials attributed to the enzymes' active site (Fe^{3+}/Fe^{2+}) transition, whereas the other at lower potentials is due to the PVP-AgNPs (Ag(0)/Ag(I)) transition.

Under aerobic conditions, introducing PZA into the reaction medium gave a catalytic voltammetric wave at the potential window of +300 mV to -800 mV (Fig. 6). This response is due to the binding of PZA to SA-CYP2E1 catalysing the low to high spin transition of iron increasing the rate of reduction of the ferric heme to ferro heme. As indicated in Fig. 7 the ferro

heme state of the enzyme binds molecular oxygen during which PZA is hydroxylated to 5-hydroxypyrazinamide.

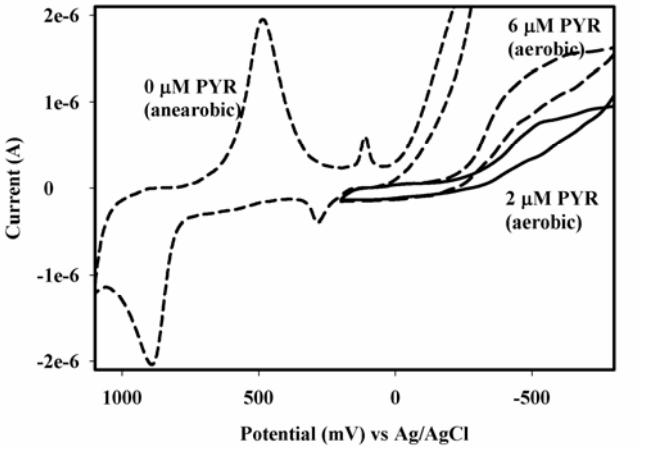

Fig. 6 CV responses in the absence and presence of PZA for the Au/PANSA/PVP-AgNPs/SA-CYP2E1 nanobiosensor

This is followed by the cleaving of the O-O bond resultant from the introduction of the second electron producing a highly active iron-oxoferryl intermediate CYP2E1 (Fe^{4+}) with 5-hydroxypyrazinoic acid as the product which is released [18], [19]. This finding was collaborated using DPV (Fig. 8). DPV responses of the Au/PANSA/PVP-AgNPs/SA-CYP2E1 nanobiosensor towards PZA indicated an increase in current with an increase in PZA concentration from 2 µM to 16 µM is observed.

The heterogeneous rate constant (k_s) of this system was calculated from the plot of E_p versus log ν according to (1).

$$\log k_s = \alpha \log(1-\alpha) + (1-\alpha)\log\alpha - \log(RT/nF\nu) - \alpha(1-\alpha)nF\Delta Ep/2.3RT \quad (1)$$

$$I_{p,c} = n^2F^2A\Gamma^*\nu/4RT \quad (2)$$

$$I_{p,c} = (n^2F^2A\Gamma^*_{\text{PANSA}}\nu)/4RT \quad (3)$$

and determined to be 1.75 s^{-1}. From the resultant straight line, a slope; also known as electron transfer coefficient (α) of 0.53 (r^2 = 0.99) was obtained. T is the temperature, ν is the scan rate of 100 V/s, ΔE_p is the separation of peak potential of +640 mV, F is the Faradays constant and n is the number of electrons calculated to be 2. This value was calculated as the slope from the plot of $I_{p,c}$ versus ν plot according to (2) indicating a two electron reaction of SA-CYP2E1 on PANSA/PVP-AgNPs. Γ^* is the amount of electroactive CYP2E1, $I_{p,c}$ is the cathodic peak current, A is the area of the electrode, R is the gas constant and Q is the quantity of charge. According to (3), the average coverage of SA-CYP2E1 on the surface of the modified electrode was estimated to be 8.25 x 10^{-5} mol cm^{-2} and 4.56 x 10^{-5} mol cm^{-2} for the Au/PANSA/AgNPs electrode.

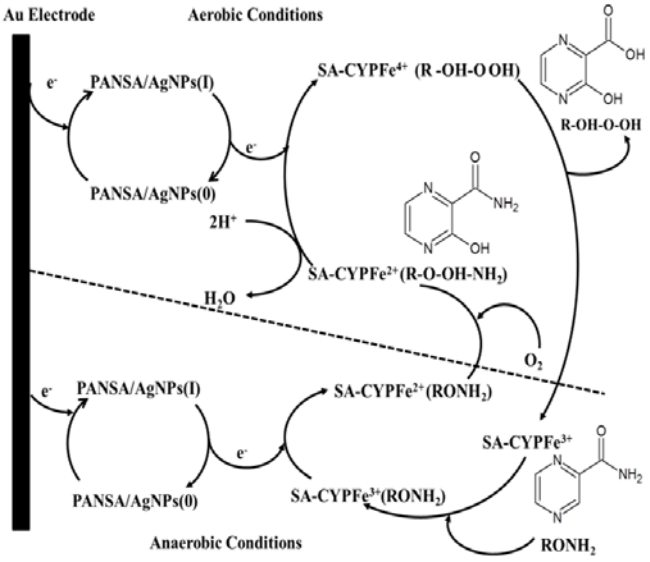

Fig. 7 Reaction scheme showing the metabolism of PZA using the Au/PANSA/PVP-AgNPs/SA-CYP2E1 nanobiosensor

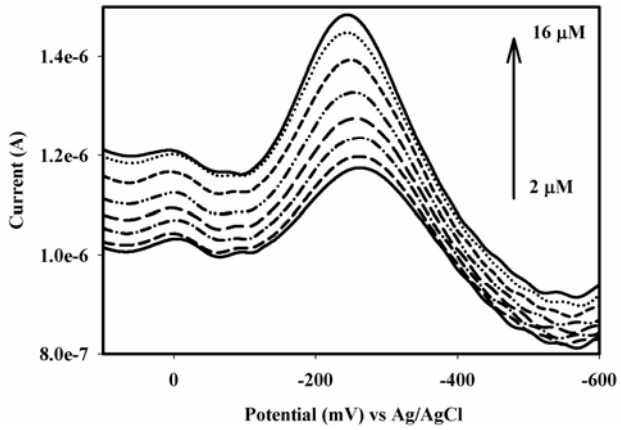

Fig. 8 DPV responses in the absence and presence of PZA for the Au/PANSA/PVP-AgNPs/SA-CYP2E1 nanobiosensor

The nanobiosensor response time was evaluated from steady state amperometry experiments performed at -300 mV (Fig. 9) where the PANSA/PVP-AgNPs/SA-CYP2E1 nanobiosensor was used as the working electrode in an air-saturated buffer cell solution while stirring was maintained at 650 rpm. The detection limit of the nanosensor was estimated to be 0.044 µM and the response times was estimated to be 30 sec. The Michaelis-Menten parameters; K_M, K_M^{app} and I_{MAX} were estimated and determined to be 6.0 µM, 1.41 µM and 1.51 x 10^{-6} µA, respectively, while a sensitivity of 1.38 µA/µM was estimated from the calibration curve (Fig. 10).

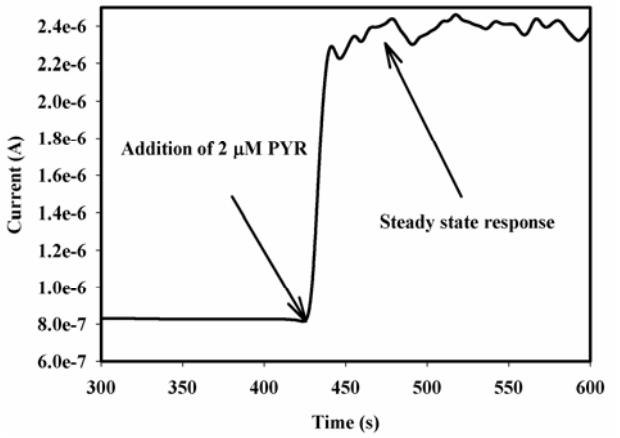

Fig. 9 Steady state amperometric response of the Au/PANSA/PVP-AgNPs/SA-CYP2E1 nanobiosensor

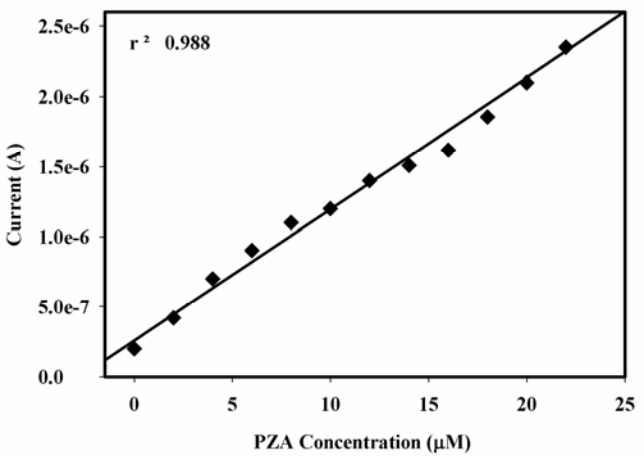

Fig. 10 Calibration curve of the Au/PANSA/PVP-AgNPs/SA-CYP2E1 nanobiosensor

IV. Conclusion

A simple yet effective electrochemical technique is illustrated for the determination of the TB drug pyrazinamide at the Au/PANSA/PVP-AgNPs/SA-CYP2E1 modified electrode. The nanocomposite provided a suitable platform for CYP2E1 attachment facilitating the catalytic reduction of PZA. Finally, the blood peak concentration of PZA (50µg/mL or 0.050µM) occurring 2 h after administration of a 200 mg PZA dose, is within the dynamic linear response range of the nanobiosensor (0.044-16µM) indicating that the nanobiosensor proposed here can be used successfully in serum.

Acknowledgment

The SensorLab of the University of the Western Cape, South Africa and The National Research Foundation of South Africa are greatly acknowledged for financing the completion of this study.

References

[1] M. Zimic, P. Fuentes, R.H. Gilman, A.H. Gutiérrez, D. Kirwan and P. Sheen P, ''Pyrazinoic Acid Efflux Rate in Mycobacterium Tuberculosis is a better proxy of Pyrazinamide Resistance,'' *Tuberculosis* (Edinb), vol. 92, no.1, pp. 84–91, January 2012.

[2] T. Sahota and O.D. Pasqua, ''Feasibility of a Fixed-Dose Regimen of Pyrazinamide and its Impact on Systemic Drug Exposure and Liver Safety in Patients with Tuberculosis,'' *Antimicrob. Agents Chemother*., vol. 56, no. 11, pp. 5442-5449, November 2011.

[3] Y. Zhang, A. Scorpio, H. Nikaido and Z. Sun, ''Role of Acid pH and Defficient Efflux of Pyrazinoic Acid in Unique Susceptibility of Mycobacterium tuberculosis to Pyrazinamide,'' *J. Bacteriol.,* vol. 181, no.7, pp 2044-2049, April 1999.

[4] M. Salfinge, and L.B. Heifets, ''Determination of Pyrazinamide MICs for mycobacterium tuberculosis at Different pHs by the Radiometric Method,'' *Antimicrob. Agents Chemot*., vol. 32, no. 7, pp.1002-1004, July 1988.

[5] Y. Zhang, and D. Mitchison, ''The Curious characteristics of pyrazinamide: a review.'' *Int. J. Tuberc. Lung Dis*., vol. 7, 1, pp 6-21, January 2003.

[6] Y. Zhang, M. W. Wade, A. Scorpio, H. Zhang, and Z. Sun, ''Mode of Action of Pyrazinamide: disruption of Mycobacterium tuberculosis membrane transport and energetics by pyrazinoic acid,'' *J. Antimicrob. Chemother.*, vol. 52, 5, pp. 790-795, November 2003.

[7] P. Lu, A.C. Haagsma, H. Pham, J.J.Maaksant, S. Mol, H. Lill, and D. Bald, ''Pyrazinoic Acid Decreases the Proton Motive Force, Respiratory ATP Synthesis Activity, and Cellular ATP Levels,'' *Antimicrob. Agents Chemother.*, vol. 55, no. 11, pp. 5354-5357, November 2011.

[8] T. Gumbo, C.S. Dona, C. Meek, and R. Leff, ''Pharmacokinetics-Pharmacidynamics of Pyrazinamide in a Novel In Vitro Model of Tuberculosis for Sterilizing Effect: a Paradigm for Faster Assessment of New Antituberculosis Drugs,'' *Antimicrob. Agents Chemother*., vol. 53, no. 8, pp. 3197-3204, August 2009.

[9] W.Shi, X. Zhang, X. Jiang, H. Vuan, J.S. Lee, C.E. Barry 3rd, H. Wang, W. Zhang, and Y. Zhang, ''Pyrazinamide Inhibits Trans-Translation in Mycobacterium tuberculosis,'' *Science*, vol. 333, no 6049, pp.1630-1632, September 2011.

[10] S.T. Cole, ''Pyrazinamide- Old TB Drug Finds New Target,'' *Science*, vol. 333, no.6049, pp. 1583-1584, September 2011.

[11] W. Bleibel, S. Kim, and K. D'Silva, ''Drug-Induced Liver Injury: Review Article,'' *Did. Dis. Science.,* vol. 52, pp. 2463-2471, March 2007.

[12] K. C. Chang, C. C. Leung, W. W. Yew, T. Y. Lau, and C.M. Tam, ''Hepatotoxicity of Pyrazinamide,'' *Am. J. Respir. Crit. Care Med*., vol. 177, no.12, pp. 13911397, June 2013.

[13] R. F. Ngece, N. West, P. M. Ndangili, and E. I. Iwuoha, ''A silver Nanoparticle/Poly (8-Anilino-1-Naphthalene Sulphonic Acid) Bioelectrochemical Biosensor System for the Analytical Determination of Ethambutol,'' *Int. J. Electrochem. Sc.,* vol.6, pp. 1820-1834, June 2011.

[14] H. Eoh, and P. J. Brennan, ''The Mycobacterium tuberculosis MEP (2C-methyl-D-erythritol 4-phosphate) pathway as a new drug target,'' *Tuberculosis*, vol. 89, no. 1, pp.1-11, January 2011.

[15] W. C. Wang, J. Y. Chen, Y. K. Chen, and L. M. Lin, ''Tuberculosis of the head and neck: a review of 20 cases,'' *Oral Surg. Oral Med. Oral Pathol. Oral Radiol. Endod.*, vol. 107, no. x, pp. 381-382, month 2009.

[16] Y. Yin Zhou and L. Zhu, ''Electrochemical behavior of bisphenol A at glassy carbon electrode modified with gold nanoparticles, silk fibroin, and PAMAM dendrimers,'' *Microchim. Acta,* vol.170, no. 3, pp. 100–105, March 2010.

[17] Ding H. Hongbo, and S-M. Park, ''Electrochemistry of Conductive Polymers XXVII. Effects of Polystyrene Sulfonate on Electrochemical Behavior of Polyaniline,'' *Int. J. Electrochem. Sc.,* vol.150, no. 2, pp. E34-E38, January 2002.

[18] T. Yamamoto, Y. Moriwaki, and K. Higashino, ''Study of the metabolism of pyrazinamide using a high-performance liquid chromatographic analysis of urine samples,'' *Anal. Biochem*., vol. 160, no.2, pp. 346-349, February 1987.

[19] A. Mehmedagic, P. Verite, S. Menager, D. Andre, and O. Lafont, ''Determination of pyrazinamide and its main metabolites in rat urine by high-performance liquid chromatography,'' *J. Chromatogr. B Biomed. Sci. Appl*., vol. 695, no, 2, pp. 365-372, August 1997.